ACS APPLIED NANO MATERIALS

www.acsanm.org Article

Waved 2D Transition-Metal Disulfides for Nanodevices and Catalysis: A First-Principle Study

Youchao Kong, Haoqiang Ai, Wei Wang, Xiuhua Xie, Kin Ho Lo, Shuangpeng Wang,* and Hui Pan*

Cite This: *ACS Appl. Nano Mater.* 2020, 3, 2804−2812 Read Online

ACCESS | Metrics & More | Article Recommendations | Supporting Information

ABSTRACT: Two-dimensional (2D) transition-metal dichalcogenides (TMDs) monolayers have found various applications spanning from electronics in physics to catalysis in chemistry due to their unique physical and chemical properties. Here, the effect of structure engineering on the physical and chemical properties of transition-metal disulfide monolayers (MS_2) is systematically investigated based on density functional theory (DFT) calculations. The calculation results show that waved MS_2 (w-MS_2) can be achieved under compression due to the zero in-plane stiffness, leading to high flexibility within a wide range of compression. The bandgap and conductivity of semiconducting w-MS_2 are reduced because the d orbitals of transition-metal elements become more localized as the curvature increases. A transition from a direct band to an indirect one is observed in w-MoS_2 and w-WS_2 after a critical strain. We further demonstrate the structure engineering can modulate the magnetism of w-VS_2, leading to nonuniform distribution of magnetic moments along the curvature. Furthermore, we find that waved TMDs show reduced Gibbs free energy for hydrogen adsorption, resulting in enhanced catalytic performance in hydrogen reaction evolution (HER). It is expected that the waved 2D TMDs may find applications into various areas, such as nanodevices and catalysis.

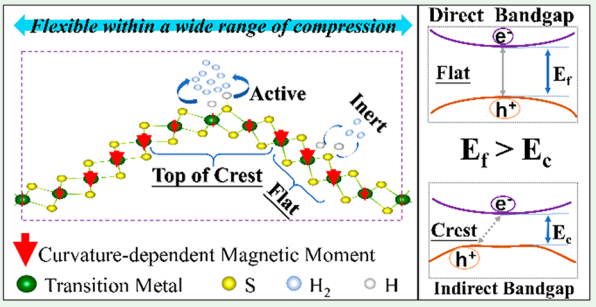

KEYWORDS: *waved 2D materials, transition-metal disulfides, strain engineering, electronic and magnetic properties, hydrogen evolution reaction, DFT calculations*

INTRODUCTION

Since the discovery of graphene in 2004, two-dimensional (2D) materials have triggered extensive interests in many research fields due to their excellent physical and chemical properties.[1−4] Their intriguing properties have resulted in wide applications in various areas, such as mechanics,[5,6] electronics,[7,8] photoelectronics,[9,10] and catalysts.[11,12] Among them, transition-metal dichalcogenides (TMDs) have attracted increasing attention because of their versatile and tunable properties.[13] Different from graphene, the TMD monolayer is a three-layer structure (X-M-X: M = transition metal atom, and X = chalcogen atom), which provides a lot of chances to tailor their properties for multiple applications. Various methods, such as electron and atom doping,[14,15] vacancy control,[16] deformation,[17] and thermal annealing,[18] have been used for the purpose, and amazing properties have been reported, such as valley electronics,[19] magnetism,[20] and superconductivity.[21]

The out-of-plane deformation, such as buckling,[22] wrinkling,[23] scrolling,[24] and folding,[25] is observed in many 2D materials because of their ultrathin nature, which has triggered greatly attention recently.[26,27] For instance, waved graphene had been reported to show high performance on molecule adsorption, chemical reaction, and hydrogen evolution reaction (HER).[28−33] Xie et al. reported that a spontaneous ripple superlattice was formed when a van der Waals (vdW) TMD heterostructure with large lattice mismatch was fabricated.[34] Out-of-plane deformation (or bended structure) has also been reported on other 2D TMDs.[35,36] However, to the best of our knowledge, few systematic studies have reported on their physical and chemical properties affected by the periodic curvatures. In this work, we construct waved MS_2 (M = Mo, W, Sn, and V) to investigate the effect of curvature on their physical and chemical properties using first-principles calculations. We find that these waved nanosheets show high flexibility upon compression, and their band structures depend on the compression, resulting in a transition from direct bandgap to an indirect one. The compression has no effect on the ground states of waved MS_2 but strongly affects the local magnetic moments (LMM) of magnetic w-VS_2, leading to the nonuniform distribution of magnetic moments along the curvature. We further show that the curvature can improve the catalytic activity of MS_2 for HER, which is greatly enhanced by simply increasing the compression. Our well-rounded calcu-

Received: January 14, 2020
Accepted: March 9, 2020
Published: March 9, 2020

https://dx.doi.org/10.1021/acsanm.0c00119
ACS Appl. Nano Mater. 2020, 3, 2804−2812

lation paves a way to tune the physical and chemical properties of MS_2 for versatile applications by strain engineering.

COMPUTATIONAL METHOD

All density functional theory (DFT) calculations are carried out to investigate study the physical and chemical properties of waved 2D TMDs. The Perdew−Burke−Eznerhof generalized gradient approximation (PBE-GGA) is used for the exchange-correlation energy.[37] The projector augmented wave (PAW) method in the Vienna ab initio simulation package (VASP) is employed in this work. The integration of the first Brillouin zone is carried out with the Monkhorst and Pack (MP) scheme of k-point sampling. A 7 × 1 × 1 MP grid is used for the k-point sampling during relaxation calculation, while a 21 × 3 × 1 MP grid was adopted to calculate the densities of states (DOSs). A vacuum region of 15 Å is applied along the z axis to avoid the interaction between adjacent interlayers. All the calculations use 1.0×10^{-6} eV/atom as total energy convergence condition and 0.04 eV/A as maximum force convergence criteria, which are carefully tested before the further calculation. Spin-polarization is considered when calculating magnetic materials. The cutoff energy for the planar-wave expansion is set to 500 eV.

Geometrical Structures. The MS_2 monolayers are first relaxed under zero strain (Table 1) and then compressed to form waved MS_2 (w-MS_2) under various compressions (from 2% to 16%) (Figure 1). Table 1 shows the considered lengths (C_0) of planar MS_2 (p-MS_2). Under applied strain, MS_2 shows out-of-plane deformation and the wavelength shrinks (C) as compression increases (Figure S1). We investigated the w-MS_2 with various wavelengths to figure out the effects of periodic curvature on the intrinsic properties of 2D materials for potential applications in mechanics, electronics, magnetics, and catalysis.

Table 1. Optimized Geometrical Parameters and the Relative Calculated Phase of MS_2 Monolayers[a]

2D MS_2	lattice constant (a_0 = b_0) (Å)	bond length of M−S (Å)	angle of S−M−S (deg)	length of supercell C_0 (Å)	Calculated Phase
MoS_2	3.185	2.412	82.617	33.094	2H
WS_2	3.181	2.416	82.345	33.064	2H
VS_2	3.167	2.353	84.590	32.914	2H
SnS_2	3.699	2.598	90.828	38.450	1T

[a](H = Hexagonal, T = Trigonal).

Formation of w-MS_2. To indicate the possibility for the formation of the waved 2D TMDs under compression, the energy difference between waved and planar 2D monolayers is calculated first as,

$$E_{dif} = (E(\text{w-MS}_2) - E(\text{p-MS}_2))/N_u \quad (1)$$

where E(w-MS_2) and E(p-MS_2) refer to the total energies of the w- and p-MS_2 under same compression, respectively. N_u represents the total number of unit cells in a supercell. The waved supercell includes 12 unit cells and is considered in our study. We introduce the strain by shortening the wavelength (C) in the armchair direction. The strain is calculated to be $\sigma = (C_0 - C)/C \times 100\%$.

Mechanic Parameters. The mechanic parameters are obtained by following equations,[28]

$$E_s(\sigma) = (E(\text{w-MS}_2) - N_u E(\text{MS}_2))/N_u \quad (2)$$

$$F_{ten} = -\frac{\partial E_s(\sigma)}{\partial C} \quad (3)$$

$$\gamma_{ten} = -\frac{\partial F_{ten}}{\partial C} \quad (4)$$

$$C_s = -\frac{\partial^2 E_s(\sigma)}{S_0 \partial \sigma^2} \quad (5)$$

where $E(MS_2)$ is the energy of a unit cell. $E_s(\sigma)$, F_{ten}, and γ_{ten} are the strain energy, tension force, and force constant at a given strain. The in-plane stiffness (C_s) is calculated using the equilibrium area of the supercell (S_0) because of the ambiguous definition of Young's modulus of honeycomb structures.[38]

Magnetic Coupling. The magnetic ground state of w-VS_2 is determined by calculating the total energies of ferromagnetic (FM) and antiferromagnetic (AFM) states. The energy

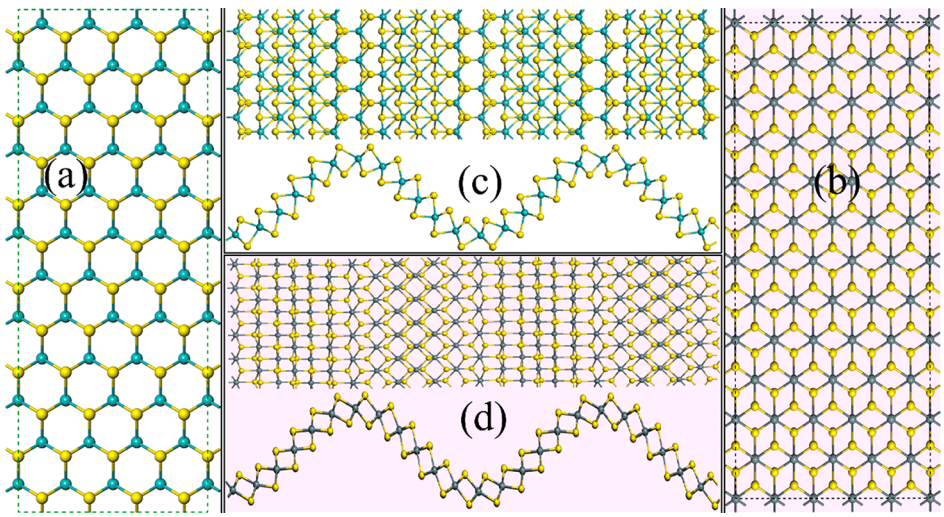

Figure 1. Structures of (a) 2H p-MS_2 and (b) 1T p-MS_2 without compression. The top and side views of (c) 2H waved MS_2 and (d) 1T waved MS_2 along the armchair direction.

https://dx.doi.org/10.1021/acsanm.0c00119
ACS Appl. Nano Mater. 2020, 3, 2804−2812

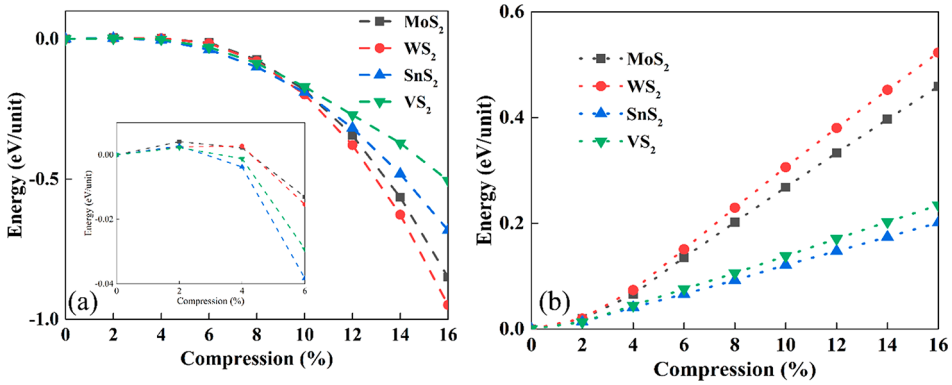

Figure 2. (a) Energy difference between planar and waved of MS_2 at same compression as calculated from eq 1. (b) Strain energy of waved MS_2 as a function of compression as calculated from eq 2.

difference between the two states (exchange energy) tells the ground state and magnetic coupling, which is expressed as,

$$E_{ex} = (E(\mathrm{AFM}) - E(\mathrm{FM}))/N_u \quad (6)$$

where E_{ex} is the exchange energy. $E(\mathrm{AFM})$ and $E(\mathrm{FM})$ are the total energies of ferromagnetic and antiferromagnetic states, respectively.

Hydrogen Evolution Reaction. The adsorption of the H atom is the first step for water splitting. The hydrogen adsorption energy is defined as,

$$\Delta E_H = E(\text{w-}MS_2 + H) - E(\text{w-}MS_2) - \frac{1}{2}E(H_2) \quad (7)$$

where $E(\text{w-}MS_2 + H)$ and $E(\text{w-}MS_2)$ represent the total energies of w-MS_2 with and without one adsorbed H, respectively. $E(H_2)$ is the energy of H_2 molecule in gas phase.

Generally, we can evaluate the HER catalytic ability by calculating Gibbs free energy, which indicates the adsorption of reactive intermediates on a catalyst based on the Sabatier principle[39] and is expressed as,[40]

$$\Delta G_H = \Delta E_H + \Delta E_{ZPE} - T\Delta S_H \quad (8)$$

$$\Delta S_H \cong -\frac{1}{2}S^0_{H_2} \quad (9)$$

where $S^0_{H_2}$ is the entropy of hydrogen molecules in the gas phase under standard conditions. ΔE_{ZPE} is the difference in zero-point energies between the adsorbed H and H in gas phase. $\Delta E_{ZPE} - T\Delta S_H$ is calculated to be 0.24 eV. Hence, eq 8 is simplified to,

$$\Delta G_H = \Delta E_H + 0.24 \quad (10)$$

RESULTS AND DISCUSSION

Structural Stability and Mechanical Properties. The structural stability of w-MS_2 is investigated first to determine their formation possibility. Figure 2a shows the energy difference (eq 1) between w-MS_2 and p-MS_2 at the same compression. As a whole, the four monolayers show the same trend; that is, the energy difference decreases negatively with the increment of compression, manifesting that the energy of the waved one is lower than that of its planar counterpart (Figure S2). Although there is a slight increment when $\sigma \leq 2\%$ (Figure 2a, inset), the amount is negligible. As the compression exceed 2%, the total energies of w-MS_2 present linear increment, while p-MS_2 shows a parabolic behavior in the increase of energy as the external strain increases (Figure S2). Clearly, the waved 2D materials start to form after $\sigma \geq 4\%$ because the energy of w-MS_2 is less than that of p-MS_2. Especially, w-SnS_2 has the largest energy difference at $\sigma = 4\%$, indicating it is easy to be bended at low compression. WS_2 shows the largest energy difference after $\sigma > 10\%$, indicating that w-WS_2 can be achieved at high compression, which is consistent with the literature.[34,41] The calculated energies indicate that the monolayer has a large probability of being buckled rather than keeping planar under compression, which is similar to graphene.[30]

The calculated strain energies of w-MS_2 (Figure 2b) increase with the reduction of the wavelength (or the increment of curvature). Figure S3 shows the bond length of S−M and angle of S−M−S at the crest and trough of w-MS_2. The angle of S−M−S goes up on the crest and goes down in the trough with the compression increasing because the crest and trough experience opposite strains, that is, tension and compression, respectively. The change of the S−M bond shows a same trend with that of the S−M−S angle (Figure S3). It is noted that the differences of the S−M−S angle and S−M bond between at the crest (or trough) of w-MS_2 and at the basal plan of p-MS_2 are up to ∼18 degrees and ∼5% at $\sigma = 16\%$, respectively. By further increasing compression, the chemical bond or bond angle cannot sustain within a reasonable range, leading to the breakdown. Hence, the compression is limited to 16% in our considered systems.

The calculated tension forces are 1.09, 0.47, 0.46, and 1.26 eV/Å for w-MoS_2, w-VS_2, w-SnS_2, and w-WS_2, respectively, which are higher than that of waved graphene (∼0.3 eV/Å), indicating that they are relatively difficult to be buckled under low compression and easy to breakdown under high compression. The result is in well agreement with the previous report on graphene.[31] w-MS_2 can be only formed after $\sigma \geq 4\%$, while waved graphene can be formed at $\sigma \geq 1\%$. Waved graphene can stably exist under large compression up to over 50%, while w-MS_2 will break at high compression. Accordingly, the calculated stiffness shows a trend of WS_2 > MoS_2 > VS_2 > SnS_2 > graphene, which is in an agreement with previous experimental results.[42−44] According to eq 5, the in-plane stiffness of w-MS_2 is zero because the strain energy is linearly proportional to the compression (Figure 2b).[38] Our calculations show that w-MS_2 is quite flexible and can be back to the basal structure after external force is released. Among these four materials, especially, SnS_2 shows the highest force tolerance due to lowest tension force, which can be

https://dx.doi.org/10.1021/acsanm.0c00119
ACS Appl. Nano Mater. 2020, 3, 2804−2812

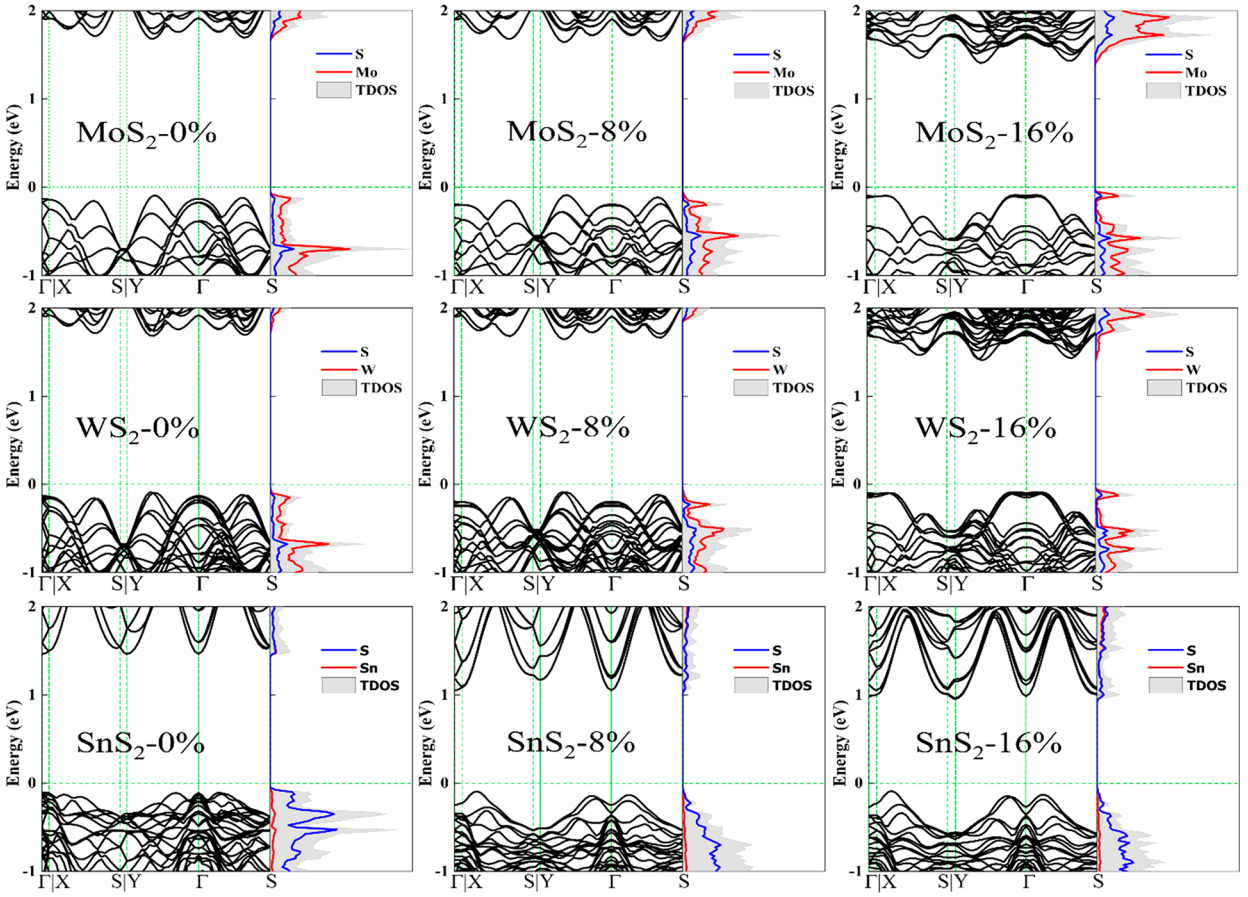

Figure 3. Calculated band structure of w-MS_2 at compressions of 0%, 8%, and 16%, respectively. The Fermi level is aligned to 0 eV.

attributed to its large lattice constant (Table 1). Additionally, we carried out molecular dynamic simulations on w-MS_2 to further confirm its stability at a compression of 16%. We found that the energy and structure kept unchanged over time (Figures S11 and S12), indicating that they are stable under high compression.

Electronic Properties. Our calculations show that the waved TMDs are highly possible to be obtained under compression. Definitely, their electronic properties will be affected by the periodic curvature. Therefore, the band structures and densities of states (DOSs) of w-MS_2 were calculated. As 2H-VS_2 has a quite narrow bandgap (~18 meV) based on the GGA-PBE calculation, we focused on the effect of curvature on the band structure of other semiconducting w-MS_2 that have large bandgaps. We see that all semiconducting w-MS_2 (Figure 3) show similar behavior in the change of band structures under compression; that is, the valence band tops (VBTs) of w-MS_2 are obviously affected under large compression. The VBTs of w-MoS_2 and w-WS_2 gradually shift along YΓ direction, that is, from one-third of YΓ to two-thirds of YΓ. Particularly, the VBTs are almost flattened under high compression. The VBT of w-SnS_2 shifts from two-thirds YΓ point to one-third of XS, while the conduction band bottom (CBB) is transferred from Γ to Y point. We further analyzed the projected band structures of the waved MS_2 (Figures S4−S6). For MoS_2, the three orbitals (Mo-$d_{x^2-y^2}$, Mo-d_{z^2}, and Mo-d_{xz}) mainly attribute to the VBT near Fermi level. At σ = 0%, the $d_{x^2-y^2}$ occupies the VBT. As the strain increases, the $d_{x^2-y^2}$ shifts gradually to low energy level, while the d_{z^2} electrons prefer the VBT, resulting in the change of VBT. When $\sigma \geq$ 12%, the VBT with a flat top appears at Γ point, resulting in a localized DOS near the Fermi level (Figure 3). The localized DOS has a large effective mass of holes, which would reduce the hole mobility and conductivity of w-MoS_2. w-WS_2 shows a same trend to w-MoS_2 due to the similar geometrical parameters between MoS_2 and WS_2 (Table 1; Figure 2) and the same valence electron structures of Mo and W. Compared with the d bands of w-MoS_2 and w-WS_2, there is no significant change in the S−p_i orbitals (S−p_i, i = x, y, z) (Figure S6). Different from w-MoS_2 and w-WS_2, the projected bands of w-SnS_2 show that the S−p_i states dominate its VBT and CBB (Figure 3). Especially, p_z shrinks to high energy level and p_x at one-third XS point occupies the top of VBT when σ ≥ 2% (Figure S6), which could be attributed to the difference of ground-state electron distribution between full d-orbit Sn ($4d^{10}$) and half d-orbit W/Mo ($4d^5$).

Moreover, we calculated the change of bandgap as the compression increases (Figure 4). The bandgap of w-SnS_2 decreases with the shortening of the wavelength except for σ = 10%, where it slightly increased, due to the slight decrease of VBT (Figure S6; 10%). w-SnS_2 keeps an indirect-bandgap nature under compression. For w-MoS_2 and w-WS_2, the effect of compression on their bandgaps is relatively weak, except at high compression, which leads to the reduction of the bandgap. Interestingly, a transfer from a direct to indirect band is observed at a critical compression, which is 4% for w-MoS_2 and 2% for w-WS_2 (Figure 4), respectively. Most recently, the direct-to-indirect band transitions on deformed 2D WS_2, MoS_2, and WSe_2 were observed in experiments,[46] which is in an agreement with our prediction. This transition can not only

https://dx.doi.org/10.1021/acsanm.0c00119
ACS Appl. Nano Mater. 2020, 3, 2804−2812

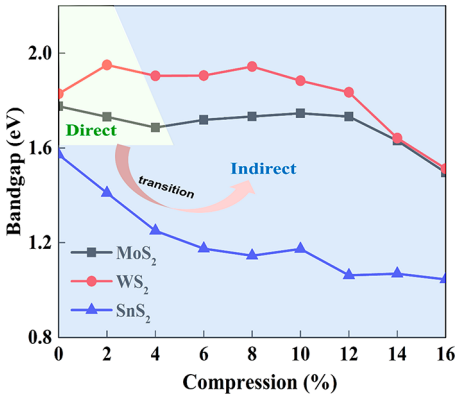

Figure 4. Calculated bandgap of w-MS_2 tuned by compression from 0% to 16%.

be used in optical switching and optical communication[45] but also would impact the efficiency of photocatalysis.[47,48]

Magnetic Property. As the electronic features of 2D materials can be tuned by controlling its structures, the magnetic property is also investigated in the same way, which may lead to intriguing phenomena and practical applications, such as data storage. Our calculations show that only w-VS_2 shows magnetism and its ground state prefers to be ferromagnetic, which is consistent with the previous report.[49] The other w-MS_2s are nonmagnetic and keep steadfast with the change of curvature (Figure S7). Therefore, we only considered the effect of curvature on the magnetism of w-VS_2. We investigated first the effect of curvature on the exchange energy (E_{ex}). Figure 5a represents the ferromagnetic and antiferromagnetic configurations. At σ = 0%, the exchange energy is about 41 meV/unit, in agreement with the previous study.[50] The positive E_{ex} indicates that p-VS_2 prefers to the ferromagnetic ground state because the energy of AFM state is higher than that of FM state. As the compression increases, we find that the calculated E_{ex} evidently decreases, leading to reduced ferromagnetic coupling. Clearly, the ferromagnetism of VS_2 is strongly affected by local curvature (Figure 5a, blue line).

Our calculation may explain the strain-induced reduction of the ferromagnetic order of VSe_2 in the epitaxial growth on some substrates.[51] We further see that the total magnetic moment of w-VS_2 supercell decreases obviously from 11.86 to 9.15 μB as the compression increases from the flat structure to the highly compressed one (Figure S7). Therefore, we investigated the variation of the magnetic moments of S and V atoms as the compression increased. The results show that the S atoms have similar magnetic moments (~0.05 μB), which are antiparallel to those of the V atoms and keep almost unchanged with the compression. However, the moment of the V atom is greatly affected by the compression (Figure 5b). To figure out the correlation between the curvature and magnetic moment, we calculate the magnetic moment of each V atom in one period of periodically waved VS_2. We mark the V atoms with the numbers from V_1 to V_{12} (Figure 5b, inset). V_7 is on the crest and V_1 is at the trough of w-VS_2. The results show that LMMs of V atoms decrease with the increase of compression, where the trend strongly depends on their positions on w-VS_2. The V_1 and V_7 contribute mostly to the reduction of total magnetic moment as their magnetic moments go down fast (from 0.9 to 0.46 μB) with the compression increasing due to the elongated S−V length and extended S−V−S angle (Figure S3). The LMMs of V atoms at other positions are also more or less affected by curvature, but the reduction is less than those of V_1 and V_7. Consequently, the change of LMM affects the exchange energy, leading to the weakening of the FM state. The contribution to the total moment is in a sequence of $V_3 = V_4 = V_9 = V_{10} > V_5 = V_{11} > V_2 = V_8 > V_6 = V_{12} > V_1 = V_7$, confirming that the waved VS_2 can provide tunable local magnetic moment by controlling the compression, which would be a favorable controllable layer in 2D heterostructures.[52]

To reveal the mechanism, the partial DOSs (PDOSs) were calculated (Figure S8). On the basis of the principle of magnetism, only a half-filled orbit has a contribution to the magnetic moment. The PDOS reveals that the areas of S-up and S-down have no obvious change with the compression increasing, indicating that S has less contribution to the change of total magnetic moment. But, the PDOS of V-d indicates a transfer from the localized valence band at a high energy (Figure S8; 0%) to the distributed states at a low energy near Fermi levels (Figure S8; 16%), resulting in the reduction of total magnetic moment because of the reduced area difference between the spin-up and spin-down states.[49]

Effect to HER Catalytic Activity. The curvature not only has a strong effect on the physical properties of waved MS_2 but also on their chemistry as well. In part, we investigated the

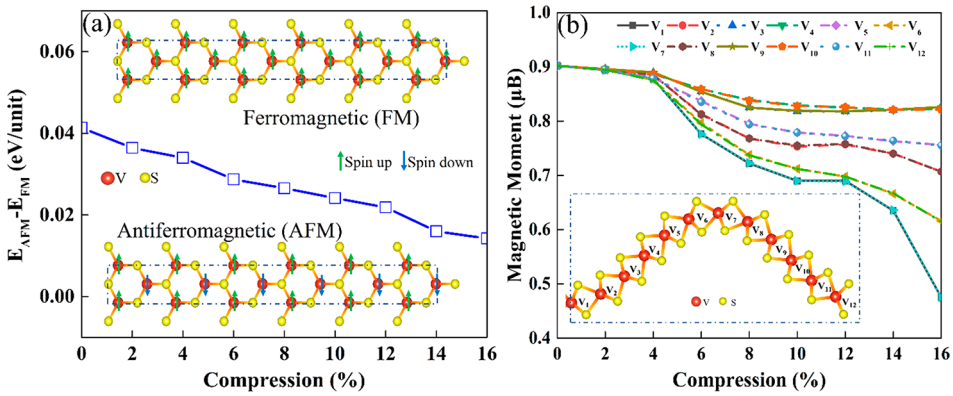

Figure 5. (a) Energy difference between AFM and FM of w-VS_2 under different compressions. The insets are top views of geometric structures for FM and AFM states. (b) Calculated magnetic moment of each V atom. The inset is the side view of monolayer 2H waved VS_2 structure with marks from V_1 to V_{12}. Dash lines indicate one supercell.

https://dx.doi.org/10.1021/acsanm.0c00119
ACS Appl. Nano Mater. 2020, 3, 2804−2812

effect of curvature on catalytic ability of w-MS_2 in HER for their applications in the electrolysis of water.[53−57] For the calculation of the Gibbs free energy (ΔG_H) of hydrogen adsorption, a large supercell with 12 × 4 unit cells is constructed. Two possible configurations for hydrogen adsorption at the crest of w-MS_2 are considered (Figure 6),

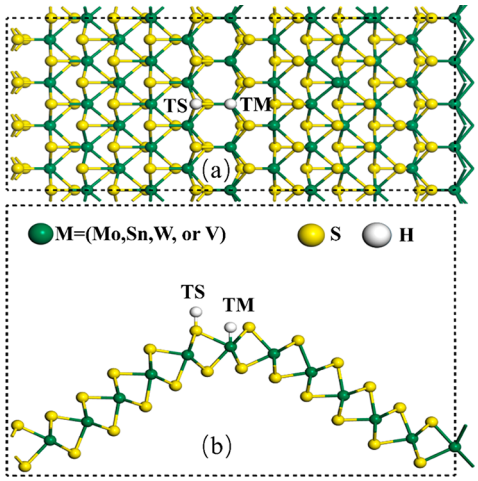

Figure 6. Representative two kinds of configurations (TS and TM) of possible H adsoption locations. (a) and (b) represent the top and side view of configurations.

that is, the top of S atom (TS) and top of transition-metal atom (TM). The relaxed structures for H-adsorbed w-MS_2 are discussed in the Supporting Information (Figures S9 and S10).

Figure 7 shows that the calculated Gibbs free energies of w-MS_2 can be tuned by controlling the compression. We see that

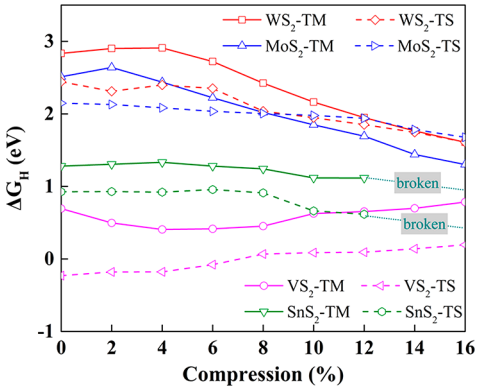

Figure 7. Calculated Gibbs free energy of waved MS_2 as the compression changes from 0% to 16%.

the TS positions are the active sites for w-WS_2, w-SnS_2 ,and w-VS_2 toward efficient HER in the whole range of considered compression due to the low Gibbs free energy. But, for w-MoS_2, the S top is active at low compression ($\sigma \leq 8\%$), while the M top becomes active at high compression ($\sigma > 8\%$). Generally, the Gibbs free energies for w-WS_2 and w-MoS_2 are reduced at high compression, leading to the enhanced HER activities. Especially, the HER performance is enhanced by 50% at $\sigma = 16\%$ for w-WS_2 and w-MoS_2. For w-SnS_2, the compression has negligible effect on the H-adsorption. Although these values are still away from thermal-neutral condition, our calculations show that the curvature can improve the HER activity by reducing the Gibbs free energy of hydrogen adsorption, which provides a fundamental understanding to observed experimental results and may guide the design of novel electrocatalysts for HER. For w-VS_2, the Gibbs free energy for H atom at TS slightly increases from −0.23 to +0.19 eV as the compression increases. The Gibbs free energy for H at the M decreases first as the compression increases ($\sigma \leq 4\%$) and then converges to the value at zero compression with further increasing strain. Compared with other absorption sites, the TM position on VS_2 shows weak binding energy after 4% due to the competitive effect from metal and surrounding S atoms as the compression varies (Figure S13). The calculated Gibbs energy indicates that VS_2 gives the best HER ($|\Delta G| < 0.2$ eV) regardless of compression. Although the improvement is not significant, we show that an optimal activity can be realized by controlling the curvature. Clearly, the HER activity of w-MS_2 follows the trend as $VS_2 > SnS_2 > MoS_2 > WS_2$.

It is noted that the strain can facilitate HER performance of w-MS_2 because the curvature produces strong local potential. Since freestanding monolayer MS_2 is believed to bend in a solvent, the local curvature must be a vital factor for the observed catalytic activity in experiment. The reduced adsorption energy and the change of adsorption position with the compression definitely affect the catalytic activity of w-MS_2 in HER.

To further understand the curvature-induced optimal HER performance of w-MS_2, we calculated the Bader charges on H at different compressions (Table S2). The larger compression, the more the net Bader charge localized on H. The accumulated charge on H would lead to the strong H adsorption. For example, for w-MoS_2, the Bader charge shows an increasing trend, which is identical to the calculated Gibbs free energy (Figure 7). Besides, we find that the optimal HER of VS_2 could be attributed to the negative Bader charge on H because it will promote the next step of the HER via the Heyrovsky mechanism: $H_{ad} + H^+ + e^- \rightarrow H_2$.[58] These results clearly indicate that curvature can facilitate HER performance due to the fast process of hydrogen adsorption and desorption.

CONCLUSIONS

In summary, we investigate systematically the physical and catalytic properties of waved MS_2 monolayer under compressions based on first-principle calculations. The result shows that the MS_2 monolayers prefer to a waved structure rather than a planar one because of low formation energy. We show that the band structure of w-MS_2 can be effectively modulated by shrinking the wavelength, such as reduced bandgap and direct-to-indirect band transfer. We further show that magnetic moment of ferromagnetic w-VS_2 is reduced as the compression increases. Interestingly, the magnetic moment of V atom strongly depends on its position on w-VS_2, which may lead to intriguing applications with position-dependent moment required. Furthermore, it is believed that the catalytic activity of w-MS_2 can be easily tuned by controlling local curvature, and we predict that high catalytic performance for HER can be achieved by structure engineering. Our calculations suggest that the structure-engineering, such as out-of-plane deformation, is a simple and effective approach to control the physical and chemical properties of 2D TMDs, which may find applications in nanodevices and catalysis.

https://dx.doi.org/10.1021/acsanm.0c00119
ACS Appl. Nano Mater. 2020, 3, 2804−2812

■ ASSOCIATED CONTENT

Supporting Information

The Supporting Information is available free of charge at https://pubs.acs.org/doi/10.1021/acsanm.0c00119.

Figures of representative structures, calculated strain energies, calculated S−M bond length and S−M−S bond angles, projected band structures, calculated magnetic moments, density of states, relaxed structures, molecular dynamics simulation, and snapshots of intermediates at different simulation times and tables of calculated S−H and M−H bonds at different compressions and calculated net Bader charge under different compressions (PDF)

■ AUTHOR INFORMATION

Corresponding Authors

Shuangpeng Wang − *MOE Joint Key Laboratory, Institute of Applied Physics and Materials Engineering and Department of Physics and Chemistry, Faculty of Science and Technology, University of Macau, Macao SAR 999078, P. R. China;* orcid.org/0000-0001-8464-4994; Email: spwang@um.edu.mo

Hui Pan − *MOE Joint Key Laboratory, Institute of Applied Physics and Materials Engineering and Department of Physics and Chemistry, Faculty of Science and Technology, University of Macau, Macao SAR 999078, P. R. China;* orcid.org/0000-0002-6515-4970; Phone: +853 88224427; Email: huipan@um.edu.mo; Fax: +853 88222454

Authors

Youchao Kong − *MOE Joint Key Laboratory, Institute of Applied Physics and Materials Engineering, University of Macau, Macao SAR 999078, P. R. China*

Haoqiang Ai − *Department of Electromechanical Engineering, Faculty of Science and Technology, University of Macau, Macao SAR 999078, P. R. China*

Wei Wang − *MOE Joint Key Laboratory, Institute of Applied Physics and Materials Engineering, University of Macau, Macao SAR 999078, P. R. China*

Xiuhua Xie − *MOE Joint Key Laboratory, Institute of Applied Physics and Materials Engineering, University of Macau, Macao SAR 999078, P. R. China; State Key Laboratory of Luminescence and Applications, Changchun Institute of Optics, Fine Mechanics and Physics, Chinese Academy of Sciences, Changchun 130033, P. R. China*

Kin Ho Lo − *Department of Electromechanical Engineering, Faculty of Science and Technology, University of Macau, Macao SAR 999078, P. R. China*

Complete contact information is available at: https://pubs.acs.org/10.1021/acsanm.0c00119

Notes

The authors declare no competing financial interest.

■ ACKNOWLEDGMENTS

This work was supported by the Science and Technology Development Fund from Macau SAR (0102/2019/A2, 0035/2019/AGJ, 084/2016/A2, 199/2017/A3, and 0125/2018/A3) and Multi-Year Research Grants (MYRG2017-00027-FST, MYRG2018-00003-IAPME, MYRG2017-00149-FST, SRG2016-00085-FST) from Research & Development Office at University of Macau. The DFT calculations were performed at High Performance Computing Cluster (HPCC) of Information and Communication Technology Office (ICTO) at University of Macau.

■ REFERENCES

(1) Novoselov, K. S.; Geim, A. K.; Morozov, S. V.; Jiang, D.; Zhang, Y.; Dubonos, S. V.; Grigorieva, I. V.; Firsov, A. A. Electric Field Effect in Atomically Thin Carbon Films. *Science* **2004**, *306*, 666−669.

(2) Han, M. Y.; Ozyilmaz, B.; Zhang, Y.; Kim, P. Energy Band-gap Engineering of Graphene Nanoribbons. *Phys. Rev. Lett.* **2007**, *98*, 206805.

(3) Turner, J. A. Sustainable Hydrogen Production. *Science* **2004**, *305*, 972−974.

(4) Li, G. Q.; Zhang, D.; Qiao, Q.; Yu, Y. F.; Peterson, D.; Zafar, A.; Kumar, R.; Curtarolo, S.; Hunte, F.; Shannon, S.; Zhu, Y. M.; Yang, W. T.; Cao, L. Y. All the Catalytic Active Sites of MoS_2 For Hydrogen Evolution. *J. Am. Chem. Soc.* **2016**, *138*, 16632−16638.

(5) Bertolazzi, S.; Brivio, J.; Kis, A. Stretching and Breaking of Ultrathin MoS_2. *ACS Nano* **2011**, *5*, 9703−9709.

(6) Castellanos-Gomez, A.; Van Leeuwen, R.; Buscema, M.; van der Zant, H. S. J.; Steele, G. A.; Venstra, W. J. Single-layer MoS_2 Mechanical Resonators. *Adv. Mater.* **2013**, *25*, 6719−6723.

(7) Lembke, D.; Bertolazzi, S.; Kis, A. Single-layer MoS_2 Electronics. *Acc. Chem. Res.* **2015**, *48*, 100−110.

(8) Pang, J.; Bachmatiuk, A.; Yin, Y.; Trzebicka, B.; Zhao, L.; Fu, L.; Mendes, R. G.; Gemming, T.; Liu, Z.; Rümmeli, M. H. Applications of Phosphorene and Black Phosphorus in Energy Conversion and Storage Devices. *Adv. Energy Mater.* **2018**, *8*, 1702093.

(9) Lee, D.; Hwang, E.; Lee, Y.; Choi, Y.; Kim, J. S.; Lee, S.; Cho, J. H. Multibit MoS_2 Photoelectronic Memory with Ultrahigh Sensitivity. *Adv. Mater.* **2016**, *28*, 9196−9202.

(10) Li, F.; Gao, F.; Xu, M. X.; Liu, X. X.; Zhang, X. K.; Wu, H. L.; Qi, J. J. Tuning Transport and Photoelectric Performance of Monolayer MoS_2 Device by E-Beam Irradiation. *Adv. Mater. Interfaces* **2018**, *5*, 1800348.

(11) Zhang, L.; Ji, X.; Ren, X.; Ma, Y.; Shi, X.; Tian, Z.; Asiri, A. M.; Chen, L.; Tang, B.; Sun, X. Electrochemical Ammonia Synthesis via Nitrogen Reduction Reaction on MoS_2 Catalyst: Theoretical and Experimental Studies. *Adv. Mater.* **2018**, *30*, 1800191.

(12) Anjum, M. A. R.; Jeong, H. Y.; Lee, M. H.; Shin, H. S.; Lee, J. S. Efficient Hydrogen Evolution Reaction Catalysis in Alkaline Media by All-in-one MoS_2 with Multifunctional Active Sites. *Adv. Mater.* **2018**, *30*, 1707105.

(13) Choi, W.; Choudhary, N.; Han, G. H.; Park, J.; Akinwande, D.; Lee, Y. H. Recent Development of Two-dimensional Transition Metal Dichalcogenides and Their Applications. *Mater. Today* **2017**, *20*, 116−130.

(14) Yang, J.; Hiroyo, K.; Wong, C. P. Y.; Goh, K. E. J. Electrical Doping Effect of Vacancies on Monolayer MoS_2. *J. Phys. Chem. C* **2019**, *123*, 2933−2939.

(15) Yang, S. Z.; Gong, Y.; Manchanda, P.; Zhang, Y. Y.; Ye, G.; Chen, S.; Song, L.; Pantelides, S. T.; Ajayan, P. M.; Chisholm, M. F.; Zhou, W. Rhenium-doped and Stabilized MoS_2 Atomic Layers with Basal-plane Catalytic Activity. *Adv. Mater.* **2018**, *30*, 1803477.

(16) Li, L.; Qin, Z.; Ries, L.; Hong, S.; Michel, T.; Yang, J.; Salameh, C.; Bechelany, M.; Miele, P.; Kaplan, D.; Chhowalla, M.; Voiry, D. Role of Sulfur Vacancies and Undercoordinated Mo Regions in MoS_2 Nanosheets toward the Evolution of Hydrogen. *ACS Nano* **2019**, *13*, 6824−6834.

(17) Hui, Y. Y.; Liu, X.; Jie, W.; Chan, N. Y.; Hao, J.; Hsu, Y. T.; Li, L. J.; Guo, W.; Lau, S. P. Exceptional Tunability of Band Energy in a Compressively Strained Trilayer MoS_2 Sheet. *ACS Nano* **2013**, *7*, 7126−7131.

(18) Li, D.; Cheng, H. C.; Wang, Y.; Zhao, Z.; Wang, G.; Wu, H.; He, Q.; Huang, Y.; Duan, X. The Effect of Thermal Annealing on Charge Transport in Organolead Halide Perovskite Microplate Field Effect Transistors. *Adv. Mater.* **2017**, *29*, 1601959.

(19) Tarasenko, S. Valley Currents Controlled by Light. *Nat. Nanotechnol.* **2014**, *9*, 752−753.
(20) Zhang, H.; Liu, L. M.; Lau, W. M. Dimension-dependent Phase Transition and Magnetic Properties of VS_2. *J. Mater. Chem. A* **2013**, *1*, 10821−10828.
(21) Cao, Y.; Fatemi, V.; Fang, S.; Watanabe, K.; Taniguchi, T.; Kaxiras, E.; Jarillo-Herrero, P. Unconventional Superconductivity in Magic-angle Graphene Superlattices. *Nature* **2018**, *556*, 43.
(22) Yang, S.; Wang, C.; Sahin, H.; Chen, H.; Li, Y.; Li, S. S.; Suslu, A.; Peeters, F. M.; Liu, Q.; Li, J.; Tongay, S. Tuning the Optical, Magnetic, and Electrical Properties of $ReSe_2$ by Nanoscale Strain Engineering. *Nano Lett.* **2015**, *15*, 1660−1666.
(23) Dai, Z.; Liu, L.; Zhang, Z. Strain Engineering of 2D Materials: Issues and Opportunities at the Interface. *Adv. Mater.* **2019**, *31*, 1805417.
(24) Cui, X.; Kong, Z.; Gao, E.; Huang, D.; Hao, Y.; Shen, H.; Di, C.; Xu, Z.; Zheng, J.; Zhu, D. Rolling up Transition Metal Dichalcogenide Nanoscrolls via One Drop of Ethanol. *Nat. Commun.* **2018**, *9*, 1301.
(25) Annett, J.; Cross, G. L. W. Self-assembly of Graphene Ribbons by Spontaneous Self-tearing and Peeling from a Substrate. *Nature* **2016**, *535*, 271−275.
(26) Deng, S.; Berry, V. Wrinkled, Rippled and Crumpled Graphene: An Overview of Formation Mechanism, Electronic Properties, and Applications. *Mater. Today* **2016**, *19*, 197−212.
(27) Yang, L. S.; Niu, T. X.; Zhang, H.; Xu, W. J.; Zou, M. C.; Xu, L.; Cao, G. X.; Cao, A. Y. Self-assembly of Suspended Graphene Wrinkles with High Pre-tension and Elastic Property. *2D Mater.* **2017**, *4*, No. 041001.
(28) Wang, Y.; Yang, R.; Shi, Z. W.; Zhang, L. C.; Shi, D. X.; Wang, E.; Zhang, G. Y. Super-Elastic Graphene Ripples for Flexible Strain Sensors. *ACS Nano* **2011**, *5*, 3645−3650.
(29) Wang, B.; Ryu, J.; Choi, S.; Song, G.; Hong, D.; Hwang, C.; Chen, X.; Wang, B.; Li, W.; Song, H. K.; Park, S.; Ruoff, R. S. Folding Graphene Film Yields High Areal Energy Storage in Lithium-Ion Batteries. *ACS Nano* **2018**, *12*, 1739−1746.
(30) Luo, J. Y.; Jang, H. D.; Huang, J. X. Effect of Sheet Morphology on the Scalability of Graphene-Based Ultracapacitors. *ACS Nano* **2013**, *7*, 1464−1471.
(31) Pan, H.; Chen, B. Ultra-flexibility and Unusual Electronic, Magnetic and Chemical Properties of Waved Graphenes and Nanoribbons. *Sci. Rep.* **2015**, *4*, 4198.
(32) Gao, G. P.; Sun, Q.; Du, A. J. Activating Catalytic Inert Basal Plane of Molybdenum Disulfide to Optimize Hydrogen Evolution Activity via Defect Doping and Strain Engineering. *J. Phys. Chem. C* **2016**, *120*, 16761−16766.
(33) Gao, G.; Jiao, Y.; Ma, F. X.; Jiao, Y. L.; Waclawik, E.; Du, A. J. Charge Mediated Semiconducting-to-metallic Phase Transition in Molybdenum Disulfide Monolayer and Hydrogen Evolution Reaction in New 1T′ Phase. *J. Phys. Chem. C* **2015**, *119*, 13124−13128.
(34) Xie, S.; Tu, L.; Han, Y.; Huang, L.; Kang, K.; Lao, K. U.; Poddar, R.; Park, C.; Muller, D. A.; DiStasio, R. A.; Park, J. Coherent, Atomically Thin Transition-Metal Dichalcogenide Superlattices With Engineered Strain. *Science* **2018**, *359*, 1131−1136.
(35) Chen, W.; Gui, X.; Yang, L.; Zhu, H.; Tang, Z. Wrinkling of Two-Dimensional Materials: Methods, Properties and Applications. *Nanoscale Horiz.* **2019**, *4*, 291−320.
(36) Xiong, S.; Cao, G. Bending Response of Single Layer MoS_2. *Nanotechnology* **2016**, *27*, 105701.
(37) Blöchl, P. E. Projector Augmented-wave Method. *Phys. Rev. B: Condens. Matter Mater. Phys.* **1994**, *50*, 17953.
(38) Ataca, C.; Sahin, H.; Akturk, E.; Ciraci, S. Mechanical and Electronic Properties of MoS_2 Nanoribbons and Their Defects. *J. Phys. Chem. C* **2011**, *115*, 3934−3941.
(39) Laursen, A.; Varela, A.; Dionigi, F.; Fanchiu, H.; Miller, C.; Trinhammer, O.; Rossmeisl, J.; Dahl, S. Electrochemical Hydrogen Evolution: Sabatier's Principle and the Volcano Plot. *J. Chem. Educ.* **2012**, *89*, 1595−1599.
(40) Tsai, C.; Chan, K.; Abild-Pedersen, F.; Norskov, J. K. Active Edge Sites in $MoSe_2$ and WSe_2 Catalysts for the Hydrogen Evolution Reaction: A Density Functional Study. *Phys. Chem. Chem. Phys.* **2014**, *16*, 13156−13164.
(41) Hui, Y. Y.; Liu, X.; Jie, W.; Chan, N. Y.; Hao, J.; Hsu, Y. T.; Li, L. J.; Guo, W.; Lau, S. P. Exceptional Tunability of Band Energy in a Compressively Strained Trilayer MoS_2 Sheet. *ACS Nano* **2013**, *7*, 7126−7131.
(42) Han, M. Y.; Ozyilmaz, B.; Zhang, Y. B.; Kim, P. Energy Band-Gap Engineering of Graphene Nanoribbons. *Phys. Rev. Lett.* **2007**, *98*, 206805.
(43) Androulidakis, C.; Zhang, K.; Robertson, M.; Tawfick, S. Tailoring the Mechanical Properties of 2D Materials and Heterostructures. *2D Mater.* **2018**, *5*, No. 032005.
(44) Deng, S.; Gao, E.; Xu, Z.; Berry, V. Adhesion Energy of MoS_2 Thin Films on Silicon-Based Substrates Determined via the Attributes of a Single MoS_2 Wrinkle. *ACS Appl. Mater. Interfaces* **2017**, *9*, 7812−7818.
(45) Li, Y.; Rao, Y.; Mak, K. F.; You, Y.; Wang, S.; Dean, C. R.; Heinz, T. F. Probing Symmetry Properties of Few-Layer MoS_2 and h-BN by Optical Second-Harmonic Generation. *Nano Lett.* **2013**, *13*, 3329−3333.
(46) Blundo, E.; Felici, M.; Yildirim, T.; Pettinari, G.; Tedeschi, D.; Miriametro, A.; Liu, B.; Ma, W.; Lu, Y.; Polimeni, A. Evidence of the Direct-to-Indirect Band Gap Transition in Strained Two-Dimensional WS_2, MoS_2, and WSe_2. *Phys. Rev. Res.* **2020**, *2*, 12024.
(47) Peng, W.; Li, Y.; Zhang, F.; Zhang, G.; Fan, X. Roles of Two Dimensional Transition Metal Dichalcogenides as Cocatalysts in Photocatalytic Hydrogen Evolution and Environmental Remediation. *Ind. Eng. Chem. Res.* **2017**, *56*, 4611−4626.
(48) Li, Y. G.; Li, Y. L.; Sac, B. S.; Ahujad, R. Review of Two-Dimensional Materials for Photocatalytic Water Splitting from A Theoretical Perspective. *Catal. Sci. Technol.* **2017**, *7*, 545−559.
(49) Zhuang, H. L.; Hennig, R. G. Stability and Magnetism of Strongly Correlated Single-Layer VS_2. *Phys. Rev. B: Condens. Matter Mater. Phys.* **2016**, *93*, No. 054429.
(50) Pan, H. Electronic and Magnetic Properties of Vanadium Dichalcogenides. *J. Phys. Chem. C* **2014**, *118*, 13248−13253.
(51) Bonilla, M.; Kolekar, S.; Ma, Y.; Diaz, H. C.; Kalappattil, V.; Das, R.; Eggers, T.; Gutierrez, H. R.; Phan, M.-H.; Batzill, M. Strong Room-Temperature Ferromagnetism in VSe_2 Monolayers on van der Waals Substrates. *Nat. Nanotechnol.* **2018**, *13*, 289−293.
(52) Song, W. L.; Guan, X. T.; Fan, L. Z.; Cao, W. Q.; Wang, C. Y.; Zhao, Q. L.; Cao, M. S. Magnetic and Conductive Graphene Papers toward Thin Layers of Effective Electromagnetic Shielding. *J. Mater. Chem. A* **2015**, *3*, 2097−2107.
(53) Cummins, D. R.; Martinez, U.; Sherehiy, A.; Kappera, R.; Martinez-Garcia, A.; Schulze, R. K.; Jasinski, J.; Zhang, J.; Gupta, R. K.; Lou, J.; Chhowalla, M.; Sumanasekera, G.; Mohite, A. D.; Sunkara, M. K.; Gupta, G. Efficient Hydrogen Evolution in Transition Metal Dichalcogenides via a Simple One-Step Hydrazine Reaction. *Nat. Commun.* **2016**, *7*, 11857.
(54) Liu, P. T.; Zhu, J. Y.; Zhang, J. Y.; Xi, P. X.; Tao, K.; Gao, D. Q.; Xue, D. S. P Dopants Triggered New Basal Planeactive Sites and Enlarged Interlayer Spacing in Mos_2 Nanosheets toward Electrocatalytic Hydrogen Evolution. *ACS Energy Letters* **2017**, *2*, 745−752.
(55) Chatti, M.; Gengenbach, T.; King, R.; Spiccia, L.; Simonov, A. N. Vertically Aligned Interlayer Expanded MoS_2 Nanosheets on a Carbon Support for Hydrogen Evolution Electrocatalysis. *Chem. Mater.* **2017**, *29*, 3092−3099.
(56) Guo, B.; Yu, K.; Li, H.; Song, H.; Zhang, Y.; Lei, X.; Fu, H.; Tan, Y.; Zhu, Z. Hollow Structured Micro/Nano MoS_2 Spheres for High Electrocatalytic Activity Hydrogen Evolution Reaction. *ACS Appl. Mater. Interfaces* **2016**, *8*, 5517−5525.
(57) Li, C.; Cao, Q.; Wang, F.; Xiao, Y.; Li, Y.; Delaunay, J. J.; Zhu, H. Engineering Graphene and TMDs Based van der Waals Heterostructures for Photovoltaic and Photoelectrochemical Solar Energy Conversion. *Chem. Soc. Rev.* **2018**, *47*, 4981−5037.

https://dx.doi.org/10.1021/acsanm.0c00119
ACS Appl. Nano Mater. 2020, 3, 2804−2812

(58) Heyrovsky, J. A Theory of Overpotential. *Recl. Trav. Chim. Pays-Bas* **1927**, *46*, 582−585.

https://dx.doi.org/10.1021/acsanm.0c00119
ACS Appl. Nano Mater. 2020, 3, 2804−2812